

Roles of Climate Variability on the Rapid Increases of Early Winter Haze Pollution in North China after 2010

Yijia Zhang¹, Zhicong Yin^{123*}, Huijun Wang¹²³

¹Key Laboratory of Meteorological Disaster, Ministry of Education / Joint International Research Laboratory of Climate and Environment Change (ILCEC) / Collaborative Innovation Centre on Forecast and Evaluation of Meteorological Disasters (CIC-FEMD), Nanjing University of Information Science & Technology, Nanjing 210044, China

²Southern Marine Science and Engineering Guangdong Laboratory (Zhuhai), Zhuhai, China

³Nansen-Zhu International Research Centre, Institute of Atmospheric Physics, Chinese Academy of Sciences, Beijing, China

Correspondence to: Zhicong Yin (yinzhc@163.com)

Abstract. North China experiences severe haze pollution in early winter, resulting in many premature deaths and considerable economic losses. The number of haze days in early winter (December and January) in North China (HD_{NC}) increased rapidly after 2010 but declined slowly before 2010, reflecting a trend reversal. Global warming and emissions were two fundamental drivers of the long-term increasing trend of haze, but no studies have focused on this trend reversal. The autumn SST in the Pacific and Atlantic, Eurasian snow cover and central Siberian soil moisture, which exhibited completely opposite trends before and after 2010, might had close relationships with identical trends of meteorological conditions related to haze pollution in North China. Numerical experiments with a fixed emission level confirmed the physical relationships between the climate drivers and HD_{NC} during both decreasing and increasing periods. These external drivers induced a larger decreasing trend of HD_{NC} than the observations, and combined with the persistently increasing trend of anthropogenic emissions, resulted in a realistic slowly decreasing trend. However, after 2010, the increasing trends driven by these climate drivers and human emissions jointly led to a rapid increase in HD_{NC} .

Keywords: haze, $PM_{2.5}$, trend reversal, anthropogenic emission, climate variability

1 Introduction

Haze pollution, characterized by low visibility and a high concentration of fine particulate matter ($PM_{2.5}$), has become a serious environmental and social problem in China, as haze dramatically endangers human health, ecological sustainability and economic development (Ding and Liu, 2014; Wang and Chen, 2016). Exposure to $PM_{2.5}$ was estimated to cause 4.2 million premature deaths worldwide in 2015 (Cohen et al., 2017), and in China, $PM_{2.5}$ caused up to 0.96 million premature mortalities in 2017 (Lu et al., 2019). Air pollution accounts for a loss of 1.2–3.8% of the gross national product (GNP) annually (Zhang and Crooks, 2012). The most polluted areas in China are North China (NC; 34–42°N, 114–120°E), Fenwei Plain, Sichuan Basin and Yangtze River Delta; among them, NC is the most polluted (Yin et al., 2015). Meteorological conditions characterized by low surface wind speeds and a shallow boundary layer result in stagnant air, which limits the horizontal and

31 vertical dispersion of particles and induces the accumulation of pollutants (Niu et al., 2010; Wu et al., 2017; Shi et al., 2019).
32 High relative humidity favors the hygroscopic growth of pollutants (Ding and Liu, 2014; Yin et al., 2015), and anomalous
33 ascending motions weaken the downward invasion of cold and clear air from high altitudes (Zhong et al., 2019). The
34 forecasting of meteorological conditions is more accurate on the synoptic scale, but the predictions of interannual variations
35 are not good enough. Thus, the prediction of haze is a considerable challenge.

36 Previous studies proved that the interannual to decadal variations in winter haze have strong responses to external forcing
37 factors, such as the sea surface temperature (SST) in the Pacific and Atlantic, snow cover and soil moisture (Xiao et al., 2015;
38 Yin and Wang, 2016a, b; Zou et al., 2017). Anomalies of these factors exerted their impacts to modulate local dispersion
39 conditions by atmospheric teleconnections and greatly intensified haze pollution in NC. The eastern Atlantic/western Russia
40 (EA/WR), western Pacific (WP) and Eurasia (EU) patterns served as effective atmospheric bridges linking distant and
41 preceding external factors to the anomalous anticyclonic circulations over Northeast Asia (Yin and Wang, 2017; Yin et al.,
42 2017). With enhanced anticyclonic anomalies, the haze pollution in NC was significantly aggravated by poor ventilation
43 conditions and high moisture.

44 The long-term trend of haze pollution has always been attributed to increasing human activities directly related to aerosol
45 emissions (Yang et al., 2016; Li et al., 2018). It is true that emissions are important in the formation of haze, but their role
46 varies from region to region (Mao et al., 2019). The trend of haze days in Yangtze River Delta and Pearl River Delta was
47 closely related to the trend of particle emissions (Fig. S1b, c), while a weak correlation existed in Fenwei Plain (Fig. S1d). A
48 surprising phenomenon can be seen in NC: the number of winter haze days and particle emissions showed similar trends before
49 early 1990s, but afterward, their close relationship disappeared (Fig. S1a). Many recent studies also showed that the long-term
50 trend in the haze problem has likely been driven by global warming (Horton et al, 2014; Cai et al., 2017). Weakening surface
51 winds have been reported over land in the last few decades while the global surface air temperature (SAT) has warmed
52 significantly (McVicar et al., 2012). In addition, enhanced vertical stability, which favors the accumulation of pollutants, has
53 been observed with global warming (Liu et al., 2013). However, none of the above studies focused on the change in the haze
54 trend. Over the past few decades, the global and Northern Hemispheric SAT averages generally displayed a continuous
55 warming trend, which was not exactly similar to the trend of haze days in NC (Fig. S2). It follows that haze pollution, especially
56 the change in its trend, is regulated by multiple drivers and that the long-term impacts of external forcing factors, which
57 efficiently modulate the interannual and decadal variations in haze, deserve further investigation.

58 **2 Datasets and Methods**

59 **2.1 Data description**

60 Monthly mean meteorological data from 1979 to 2018 were obtained from NCEP/NCAR reanalysis datasets ($2.5^{\circ} \times 2.5^{\circ}$),
61 including the geopotential height at 500 hPa (H500), vertical wind from the surface to 150 hPa, surface air temperatures (SAT),
62 wind speed, and special humidity at the surface (Kalnay et al., 1996). The boundary layer height (BLH, $1^{\circ} \times 1^{\circ}$) values were
63 from Interim reanalysis data (ERA-Interim) obtained from the European Centre for Medium-Range Weather Forecasts
64 (ECMWF) (Dee et al., 2011). The number of haze days was calculated from the long-term meteorological data, mainly based
65 on observed visibility and relative humidity (Yin et al., 2017). The $PM_{2.5}$ concentrations from 2009 to 2016 were acquired
66 from the US embassy, and those from 2014 to 2018 were from China National Environmental Monitoring Centre. Monthly
67 total emissions of BC, NH_3 , NO_x , OC, SO_2 , PM_{10} and $PM_{2.5}$ are obtained from the Peking University emission inventory. The
68 monthly mean extended reconstructed SST data ($2^{\circ} \times 2^{\circ}$) were obtained from the National Oceanic and Atmospheric
69 Administration (Smith et al., 2008). The monthly snow cover data were supported by the Rutgers University (Robinson et al.,
70 1993). And the monthly soil moisture data ($0.5^{\circ} \times 0.5^{\circ}$) were downloaded from NOAA's Climate Prediction Center (Huug et
71 al., 2003)

72 **2.2 GEOS-Chem description and experimental design**

73 We used the GEOS-Chem model to simulate $PM_{2.5}$ concentrations (<http://acmg.seas.harvard.edu/geos/>). The GEOS-
74 Chem model was driven by MERRA-2 assimilated meteorological data (Gelaro et al., 2017). The nested grid over Asia ($11^{\circ}S$ –
75 $55^{\circ}N$, 60 – $150^{\circ}E$) had a horizontal resolution of 0.5° latitude by 0.625° longitude and 47 vertical layers up to 0.01 hPa. The
76 GEOS-Chem model includes fully coupled O_3 - NO_x -hydrocarbon and aerosol chemical mechanisms with more than 80 species
77 and 300 reactions (Bey et al., 2001; Park et al., 2004). The $PM_{2.5}$ components simulated in GEOS-Chem include sulfate, nitrate,
78 ammonium, black carbon and primary organic carbon, mineral dust, secondary organic aerosols and sea salt. At present,
79 GEOS-Chem model has been widely used, Dang et al. (2019) showed that the simulated spatial patterns and daily variations
80 of winter $PM_{2.5}$ based on this model agree well with the observations from 2013 to 2017, available years with measured $PM_{2.5}$.
81 We selected the year of 2015, which has just begun to strengthen emission reduction, and 2017, which has launched the air
82 pollution prevention and management plan for “2+26” cities (Yin and Zhang, 2020), as two representative years to simulate
83 the actual $PM_{2.5}$ concentrations, so as to evaluate the performance of the GEOS-Chem model. The simulation results are very
84 close to the observed data (Fig. S3) with high correlation coefficients reaching 0.88 and 0.85 in 2015 and 2017, indicating this
85 model could basically reflect the change of actual $PM_{2.5}$ concentrations.

86 In this study, we designed two kinds of experiments. One was an experiment for simulating $PM_{2.5}$, and the other was a
87 composite using simulated data. The simulation had changing meteorological fields in winter from 1980 to 2018 and the fixed
88 emissions in 2010 representing a high emission level. The emissions data in 2010 were from MIX 2010 (Li et al., 2017). The
89 numerical experiment was performed to examine the variation of $PM_{2.5}$ in the meteorological parameters during 1980–2018
90 under fixed-emission scenarios.

91 The composite was conducted to analyze the differences in the simulated HD_{NC} according to the years selected for the
92 external forcing factors. Using the simulated dataset with the fixed-emission scenario was capable of eliminating the impacts
93 of emissions and simply considering the effect of the four external forcing factors. The four (two) years with the largest (Favor
94 Years) and smallest (Unfavor Years) four external forcing indices (i.e., SST_P, -1 × SST_A, Snow_c and -1 × Soil_w) were selected,
95 and the differences in the simulated HD_{NC} under these four conditions in P1 (P2) were calculated. The simulated HD_{NC} in
96 Favor Years minus the simulated HD_{NC} in Unfavor Years was calculated to analyze the effect of these four forced factors.

97 2.3 Statistical methods

98 In this study, the statistical model of fitted HD_{NC} was built based on Multiple Linear Regression (MLR). This approach,
99 a model-driven method, was ultimately expressed as a linear combination of K predictors (x_i) that could generate the least
100 error of prediction \tilde{y} (Wilks, 2011). With coefficients β_i , intercept β_0 , and residual ε , the MLR formula can be written in
101 the following form: $\tilde{y} = \beta_0 + \sum \beta_i x_i + \varepsilon$.

102 The trends calculated in this study were obtained by linear regression after a 5-year running average. This method removed
103 the interannual variation and more prominent trend characteristics. Moreover, the stage trends were calculated according to
104 the inflection point, which passed the Mann-Kendall test.

105 3 Trend change of early winter haze

106 Throughout the winter in North China, the haze pollution in early winter is the most serious (Yin et al., 2019). The number
107 of haze days in early winter (December and January) in North China (HD_{NC}) reached a remarkable inflection point in 2010
108 (Fig. 1a), passing the Mann-Kendall Test. The trend of HD_{NC} was vastly different before and after 2010: slowly decreased
109 during 1991–2010 (P1) with a rate of 4.67 days/10 yr but rapidly increased after 2010 (P2, 2010–2018) with a rate of 25.43
110 days/10 yr, both of them passing 95% t test. Recent studies generally revealed that based on observations, the number of boreal
111 winter haze days across NC had a slightly decreasing trend after 1990 (Ding and Liu, 2014; He et al., 2019; Mao et al., 2019;
112 Shi et al., 2019), which is consistent with the decreasing trend presented by the dataset in our research. Excluding year 2010
113 did not affect the change in the trend of the two periods, with a decreased rate of 3.82 days/10 yr during 1991–2009, and an
114 increased rate of 20.76 days/10 yr during 2011–2018 (passing 95% t test). In addition, Dang and Liao (2019) confirmed the
115 varying trend of HD_{NC} via simulations of the global 3-D chemical transport (GEOS-Chem) model; using the well-simulated
116 frequency of serious haze days in winter, they also revealed the abovementioned changing trend of HD_{NC}, i.e., decreasing in
117 the early stage and increasing in the later stage. To further determine the reliability of the post-2010 upward trend of HD_{NC},
118 we used hourly PM_{2.5} concentrations observed at the US embassy in Beijing from 2009 to 2017 and the PM_{2.5} concentrations
119 over North China monitored by China National Environmental Monitoring Centre from 2014 to 2018 to count the number of
120 days when the PM_{2.5} concentrations were >75 $\mu\text{g m}^{-3}$ and >100 $\mu\text{g m}^{-3}$ (Fig. 1a). These statistics also reflected the rising trend

121 after 2010, as well as the improved air quality in 2017 and a rebound in pollution in 2018. Although there was a certain gap
122 between HD_{NC} (basing on visibility and humidity) and these statistics, the two datasets revealed the same variations after 2010,
123 and the statistics confirmed the robustness of the observed HD_{NC}.

124 The above analysis substantiated the rapid aggravation of haze pollution in early winter after 2010. With regard to the
125 increase in air pollution, there is no doubt that anthropogenic emissions were the fundamental cause of this long-term variation.
126 Before the mid-2000s, the particle emissions throughout NC sustained stable growth but gradually began to decline afterward,
127 which is inconsistent with the trend of HD_{NC} or even contrary in some subperiods. The previous decreasing trend of HD_{NC} hid
128 the effects of the increased pollutant emissions; thus, people ignored the pollution problem and failed to control it in time. As
129 a consequence, the subsequent rise in HD_{NC} was extremely rapid and seriously harmed the biological environment and human
130 health. The stark discrepancy between the trends of pollutant emissions and HD_{NC} strongly indicate that anthropogenic
131 emissions were not the only factor leading to a sharp deterioration in air quality after 2010 (Wei et al., 2017; Wang 2018).
132 Therefore, an important question must be asked: in addition to human activities, what factors caused the rapidly increasing
133 trend of HD_{NC} after 2010?

134 As mentioned above, local meteorological factors could modulate the capacity to disperse and the formation of haze
135 particles, which have critical influences on the occurrence of severe haze pollution. To reveal the impacts of meteorological
136 conditions on the changing trend of HD_{NC}, the area-averaged linear trends of these meteorological factors in NC during P1 and
137 P2 were calculated, all of which exceeded the 95% confidence level (Fig. 2). In P1, the area-averaged linear trends of the
138 boundary layer height (BLH), wind speed and omega all showed significant positive trends, while specific humidity showed a
139 significant negative trend in NC; these conditions favored a superior air quality (Niu et al., 2010; Ding and Liu, 2014; Yin et
140 al., 2017; Shi et al., 2019; Zhong et al., 2019). However, the trends of these four meteorological factors completely reversed
141 in P2. Reductions in the BLH and wind speed, the enhancement of moisture, and an anomalous descending motion resisted
142 the vertical and horizontal dispersions of particles and helped more pollutants gather in relatively narrow spaces. These four
143 meteorological factors expressed an evident influence on the change trend of HD_{NC} and showed reversed trends between P1
144 and P2, similar to HD_{NC}. Furthermore, the magnitudes of the change rates of these factors were stronger in P2 than in P1 (Fig.
145 2), and HD_{NC} displayed this feature as well. The GEOS-Chem simulations with changing emissions and fixed meteorological
146 conditions failed to reproduce the change trend of haze (Dang and Liao, 2019), but with varying meteorology and fixed
147 emissions could recognize the interannual variation of haze days. We designed an experiment driven by changing
148 meteorological conditions in winter from 1980 to 2018 and fixed emissions at the relatively high 2010 level. According to the
149 technical regulation on the ambient air quality index (Ministry of Ecology and Environment of the People's Republic of China,
150 2012), a haze day was defined as a day with daily mean PM_{2.5} concentration exceeding 75 $\mu\text{g m}^{-3}$. The simulations of the
151 frequency of haze days in NC by GEOS-Chem reproduced the trend reversal of haze pollution (Fig. 1b). The simulation results

152 were highly correlated with HD_{NC} and showed the feature that the trend in P2 was stronger than that in P1, indicating that
153 meteorological conditions drove the trend change of haze pollution.

154 **4 Climate variability drove the trend reversal**

155 According to many previous studies, the variabilities of the Pacific SST, Atlantic SST, Eurasian snow cover and Asian
156 soil moisture played key roles in the interannual variations in haze pollution in NC (Xiao et al., 2015; Yin and Wang, 2016a,
157 b; Zou et al., 2017), and the associated physical mechanisms were evidently revealed. Thus, the following question is raised
158 here: did these four factors drive the trend reversal of HD_{NC} , and if so, how?

159 As shown in Figure S4a, the preceding autumn SST in the Pacific, associated with the detrended HD_{NC} , presented a
160 Pacific Decadal Oscillation (PDO)-like “triple pattern” with two significant positive regions and one nonsignificant negative
161 region (Yin and Wang, 2016a; Zhao et al., 2016). In the following research, the SST anomalies in the two positively correlated
162 regions located in the Gulf of Alaska (40–60 °N, 125–165 °W) and the central eastern Pacific (5–25°N, 160 °E–110 °W) were
163 used to represent the effects originating from the North Pacific. The area-averaged September–November SST of these two
164 regions was calculated as the SST_P index, and the correlation coefficients with HD_{NC} were 0.59 and 0.67 before and after
165 removing the linear trend during 1979–2018, respectively; both correlation coefficients were above the 99% confidence level.
166 The responses of the atmosphere to these positive SST_P anomalies were the positive phase of the EA/WR pattern and the
167 enhanced anomalous anticyclone center over NC (Yin et al., 2017; Fig. S5). Modulating by such large-scale atmospheric
168 anomalies, increased moisture, anomalous upward motion and reduced BLH and wind speed (Fig. S5) created a favorable
169 environment for the accumulation of fine particles (Niu et al., 2010; Ding and Liu, 2014; Shi et al., 2019; Zhong et al., 2019).
170 A numerical experiment based on the Community Atmosphere Model version 5 (CAM5) effectively reproduced the observed
171 enhanced anticyclonic anomalies over Mongolia and North China in response to positive PDO forcing, which resulted in an
172 increase in the number of wintertime haze days over central eastern China (Zhao et al., 2016). The trend changes of the North
173 Pacific SST were examined in P1 and P2. Consistent with the changing trend of HD_{NC} , reversed trends were also found in the
174 North Pacific, i.e., a significant negative trend during P1 and a positive trend during P2 over the two Pacific areas (Fig. 3a, b).
175 These similar trend changes suggest that the North Pacific SST might have been a major driver of the abrupt change in HD_{NC} .
176 It is clear that SST_P underwent a significant trend change around 2010 (Fig. 4a). Thus, the persistent decline in SST_P during P1
177 (at a significant rate of -0.2 °C/10 yr, passing 95% t test; Table 1) contributed to the slowly decreasing trend of HD_{NC} (Fig.
178 4a) via the modulations of SST_P on the atmospheric circulation (Fig. S5). During P2, the larger increase in SST_P at a rate of
179 2.0 °C/10 yr (passing 95% t test) dramatically drove the rapid increase in HD_{NC} .

180 Besides the triple pattern in the Pacific, two areas exhibiting significant negative correlations with HD_{NC} were examined
181 in the Atlantic (Shi et al., 2015): one located over southern Greenland (50–68 °N, 18–60 °W) and another located over the

182 equatorial Atlantic (0–15 °N, 30–60 °W; Fig. S4a). The area-averaged September–November SST of the two negatively
183 correlated regions in Atlantic was defined as the SST_A index, whose correlation coefficients with HD_{NC} were –0.55 and –0.64
184 from 1979 to 2018 before and after detrending, respectively (above the 99% confidence level). The response of atmospheric
185 circulation to these negative SST_A anomalies culminated in a positive EA/WR pattern, and the stimulated easterly weakened
186 the intensity of East Asian jet stream (EAJS) in the high troposphere (Fig. S6). Influenced by the colder SST_A, there was a
187 very obvious abnormal upward movement above the boundary layer, reducing both the BLH and the surface wind speed; thus,
188 pollutants were prone to gather, causing haze pollution (Niu et al., 2010; Wu et al., 2017; Shi et al., 2019). With a linear
189 barotropic model, Chen confirmed the important role of subtropical northeastern Atlantic SST anomalies in contributing to the
190 anomalous anticyclone over Northeast Asia and anomalous southerly winds over NC, which enhanced the accumulation of
191 pollutants (Chen et al., 2019). The spatial linear trend in the SST of both Atlantic areas changed from positive in P1 to negative
192 in P2, which was completely contrary to the trend of HD_{NC} (Fig. 3a, b). The SST_A reached an inflection point in 2010 (Fig. 4b)
193 and contributed to the falling of HD_{NC} during P1 (change rate of SST_A = 0.55 °C/10 yr, passing 95% t test) and the rising of
194 HD_{NC} during P2 (change rate of SST_A = –0.52 °C/10 yr, passing 95% t test).

195 The effect of Eurasian snow cover on the number of December haze days in NC intensified after the mid-1990s (Yin and
196 Wang, 2018). The roles of extensive boreal Eurasian snow cover were also revealed by numerical experiments via the
197 Community Earth System Model (CESM): positive snow cover anomalies enhanced the regional circulation mode of poor
198 ventilation in NC and provided conducive conditions for extreme haze (Zou et al., 2017). The correlation between the October–
199 November snow cover and HD_{NC} was significantly positive in eastern Europe and western Siberia (46–62 °N, 40–85 °E, Fig.
200 S4b), where the spatial linear trend of snow cover was consistent with that of HD_{NC}. A significant negative trend in P1 and a
201 positive trend in P2 were discovered (Fig. 3c, d). The area-averaged October–November snow cover over eastern Europe and
202 western Siberia was defined as the Snowc index, and its correlation coefficients with HD_{NC} were 0.43 and 0.54 from 1979 to
203 2018 before and after detrending, respectively (above the 99% confidence level). The features of the weakened EAJS and
204 significant anomalous anticyclone could be found clearly in the induced atmospheric anomalies associated with the positive
205 Snowc anomalies (Fig. S7). The related abnormal upward motion restricted the momentum to the surface. In addition, the
206 corresponding lower BLH and weaker surface wind speed also reduced the dispersion capacity, resulting in the generation of
207 more haze pollution (Fig. S7). The Snowc index fell slowly until 2010 (with a rate of –1.8%/10 yr, passing 95% t test) and
208 then rose rapidly (with a rate of 28.3%/10 yr, passing 95% t test) and experienced a large trend reversal in 2010, in accordance
209 with the behavior of HD_{NC} (Fig. 4c). Therefore, relying on the revealed physical mechanisms, the strengthened relationship
210 between Snowc and HD_{NC} and the tremendous increase in Snowc during P2 substantially triggered the rapid enhancement of
211 haze pollution in NC.

212 In addition to snow cover, soil moisture was another important factor affecting HD_{NC} (Yin and Wang, 2016b). The
213 September-November soil moisture and HD_{NC} were negatively correlated in central Siberia (54–70 °N, 80–130 °E; Fig. S4c).
214 The area-averaged September-November soil moisture over central Siberia was denoted as the Soilw index, whose correlation
215 coefficients with HD_{NC} were -0.57 and -0.60 from 1979 to 2018 before and after detrending, respectively (above the 99%
216 confidence level). Negative Soilw anomalies could induce a positive phase of EA/WR, and the associated anticyclonic
217 circulations occurred more frequently and more strongly (Fig. S8). Correspondingly, the local vertical and horizontal
218 dispersion conditions were limited. With increasing moisture, pollutants can more easily accumulate in a confined area. The
219 spatial linear trend of soil moisture also shifted from increasing to decreasing in 2010, opposite to the trend of HD_{NC} (Fig. 3e,
220 f). The change rate of Soilw was 38.8 mm/10 yr passing 95% t test (opposite that of HD_{NC}) during P1, and the rate of change
221 became more intense (-51.8 mm/10 yr, passing 95% t test) during P2, physically driving a similar large change in HD_{NC} (Fig.
222 4d).

223 The varying trends of these four preceding external factors jointly drove the trend reversal of HD_{NC} based on their physical
224 relationships with the haze pollution in North China. To exclude the impacts of the stage trends of these variables on the
225 physical links between the climate drivers and HD_{NC} , the correlations between these factors and HD_{NC} were explored during
226 the decreasing stage (i.e., 1979–2010) and increasing stage (2010–2018), and all of these correlations were significant (Table
227 1). Thus, the physical relationships between HD_{NC} and these four factors were long-standing and did not disappear as the trend
228 changed. These four external factors had completely opposite trends in P1 and P2. Excluding SST_A , the amplitudes of the
229 change trends of the other three indices in P2 were obviously stronger than those in P1 and were identical to those of HD_{NC}
230 (Table 1). In our study, we composited the simulations based on the GEOS-Chem model to determine the impact on haze
231 pollution of each factor under the fixed-emissions level. The years in the top 20% and the bottom 20% of the four indices (i.e.,
232 SST_P , $-1 \times SST_A$, $Snowc$ and $-1 \times Soilw$) in P1 and P2 were selected, which could remove the effects of different trends. The
233 composite differences for the four external forcing factors were significant in the selected regions and passed the Student's t
234 test (Fig. S9). The responses of simulated HD_{NC} to the original (detrended) sequences of SST_P , SST_A , $Snowc$ and $Soilw$ were
235 all positive, which are consistent with the observational results (Fig. 5). Specifically, for the four original (detrended) drivers,
236 the resulting differences in simulated HD_{NC} were 3.94 (5.28), 5.97 (5.07), 1.86 (1.86) and 6.49 (6.49) days in P1 and 4.46
237 (4.46), 4.26 (4.26), 7.54 (7.54) and 7.35 (7.35) days in P2 (Fig. 5). These differences were distinct and further confirmed that
238 each factor played a role in the occurrence of haze pollution in NC.

239 These four indices were employed to linearly fit HD_{NC} based on a multiple linear regression (MLR) model (Wilks, 2011).
240 As shown in Figure 4e, the correlation coefficient between the fitted and observed HD_{NC} was 0.82. After a five-year running
241 average, the correlation coefficient reached 0.92. This model showed good ability to fit the inflection point in 2010 and
242 highlighted the trend changes. Such a good fitting effect indicates that changes in the four external forcing factors could well

243 have influenced the variation in HD_{NC} . By exciting stronger responses in the atmosphere, such as the positive EA/WR phase
244 and the strengthened anomalous anticyclone over NC, the abovementioned climate drivers created stable and stagnant
245 environments in which the haze pollution in NC could rapidly exacerbate after 2010 (Table 1). Among the four indices, the
246 correlation coefficients between SST_P and $Snowc$ (Pair 1) and between SST_A and $Soilw$ (Pair 2) were high, while the rest were
247 insignificant. The variance inflation factors of the four factors in the MLR model were less than 2, showing that the collinearity
248 among them was weak. When selecting one factor from both Pair 1 and Pair 2 to refit HD_{NC} , the correlation coefficient between
249 the fitted and observed HD_{NC} and the trends of the fitted HD_{NC} in P2 worsened (Fig. S10). Therefore, these four external factors
250 were all indispensable to achieve a better fitting effect. The intercorrelated climate factors of Pair 1 and Pair 2 contributed
251 27.8% and 84.6%, respectively, to the trends of HD_{NC} in P1 and 54.8% and 20.4% to the trends in P2. Thus, the joint effect of
252 SST_A and $Soilw$ played a more important role in the decreasing trend of HD_{NC} in P1; however, the impacts of SST_P and $Snowc$
253 were more than twice those of SST_A and $Soilw$ in P2. More importantly, the fitted curve revealed a decreasing trend of HD_{NC}
254 (-5.24 days/10 yr, passing 95% t test) that was larger than observed (-4.67 days/10 yr) during P1. Many studies have noted
255 that human activities have led to persistently increasing trends of HD_{NC} (Yang et al., 2016; Li et al., 2018). The combination
256 of the exorbitant decreased trend indicated by climate conditions and the long-term trend from anthropogenic emissions
257 resulted in a realistic slow decline (Table 2). This proportion of the trend explained by climate drivers (72.3%) decreased in
258 P2 because the increasing trend driven by the climate drivers and emissions jointly led to a rapid increase in HD_{NC} .

259 **5 Conclusions and discussions**

260 Haze events in early winter in North China exhibited rapid growth after 2010, which was completely different from the
261 slow decline observed before 2010, showing a trend reversal in the year 2010 (Fig. 1). The trend changes of associated
262 meteorological conditions exhibited identical responses. After 2010, the lower BLH, weakened wind speed, sufficient moisture
263 and anomalous ascending motion (all with larger tendencies than before 2010) limited the horizontal and vertical dispersion
264 conditions and thus enhanced the occurrence of early winter haze pollution (Fig. 2). However, before 2010, the climate
265 conditions showed the opposite characteristics and could create an environment with adequate ventilation for the dissipation
266 of particles.

267 In this study, the external forcing factors that closely related to the significant growth of HD_{NC} after 2010 and the
268 associated physical mechanisms were investigated. These factors might strongly link to the anomalous anticyclone over NC
269 via exciting the EA/WR teleconnection pattern, thus regulating the meteorological conditions, weakening the dispersion
270 conditions and facilitating the accumulation of haze pollutants. The four climate drivers physically related to HD_{NC} showed
271 exactly opposite trend changes with an inflection point in 2010, which agrees with the behavior of HD_{NC} (Fig. 4). The factors
272 of Pair 1 (SST_A and $Soilw$) and Pair 2 (SST_P and $Snowc$) had joint effects and played more important roles in the increasing

273 trend of HD_{NC} in P2 and the decreasing trend of HD_{NC} in P1, respectively (Table 2). The fitting result of the four factors with
274 the trend of HD_{NC} showed a strongly decreasing trend in P1 and a weakly increasing trend in P2. Together with increasing
275 emissions, these factors jointly led to a relatively slow decreasing trend of HD_{NC} before 2010 and rapid growth afterward.
276 Therefore, both the decreasing trend in P1 and the increasing trend in P2 were caused by a combination of climate drivers and
277 emissions.

278 Note that a number of factors contribute to the uncertainties in our results. Although a high emission scenario was used
279 to simulate the number of haze days and emphasized the influence of meteorology, no complete and varied emission inventories
280 were used to drive the GEOS-Chem model to make a comparison, which caused certain uncertainty. Furthermore, when
281 assessing the contribution percentages of the external forcing factors, the coupling effect between climate variability and
282 anthropogenic emissions was not considered, therefore the contribution rate of climate conditions might be overestimated.

283 For the long-term trend of haze, human activities are the recognized and fundamental driver (Li et al., 2018; Yang et al
284 2016). Anthropogenic emissions have exceeded a high level since the 1990s, providing a sufficient foundation for the
285 generation of severe haze pollution (Fig. 1). However, the effects of climate variability delayed warnings before 2010. Together
286 with the local meteorological conditions, the trends of the climate drivers reversed in 2010, initiating a dramatically increase
287 in HD_{NC} after 2010, which quickened the worsening of haze pollution in NC (Fig. 4e; Table 1). The superimposed effect of
288 high-level human emissions with strengthened climate anomalies loudly sounded the alarms through the extremely rapid rise
289 of haze pollution.

290 *Data availability.* The monthly mean meteorological data are obtained from NCEP/NCAR reanalysis datasets
291 (<https://www.esrl.noaa.gov/psd/data/gridded/data.ncep.reanalysis.html>). The boundary layer height data are available from the
292 Interim reanalysis dataset (<http://www.ecmwf.int/en/research/climate-reanalysis/era-interim>). The number of haze days can be
293 obtained from the authors. The $PM_{2.5}$ concentrations from 2009 to 2016 can be downloaded from the US embassy
294 (<http://www.stateair.net/web/historical/1/1.html>), and those from 2014 to 2018 can be downloaded from China National
295 Environmental Monitoring Centre (<http://beijingair.sinaapp.com/>). The monthly total emissions of BC, NH_3 , NO_x , OC, SO_2 ,
296 PM_{10} and $PM_{2.5}$ are obtained from the Peking University emission inventory (<http://inventory.pku.edu.cn/>). SST data are
297 downloaded from <http://www.esrl.noaa.gov/psd/data/gridded/data.noaa.ersst.v4.html>. Soil moisture data are obtained from
298 <https://www.esrl.noaa.gov/psd/data/gridded/data.cpcsoil.html>. Snow cover data can be downloaded from Rutgers University:
299 <http://climate.rutgers.edu/snowcover/>. The emissions of 2010 can be downloaded from
300 <http://geoschemdata.computecanada.ca/ExtData/HEMCO/MIX>.

301 **Acknowledgements**

302 This work was supported by the National Key Research and Development Plan (2016YFA0600703), National Natural Science
303 Foundation of China (41705058, 41991283 and 91744311), and the funding of Jiangsu innovation & entrepreneurship team.

304 **Author contributions**

305 Wang H. J. and Yin Z. C. designed the research. Yin Z. C. and Zhang Y. J. performed research. Zhang Y. J. prepared the
306 manuscript with contributions from all co-authors.

307 **Competing interests**

308 The authors declare no conflict of interest.

309 **References**

- 310 Bey, I., Jacob, D. J., Yantosca, R. M., Logan, J. A., Field, B. D., Fiore, A. M., Li, Q. B., Liu, H. G. Y., Mickley, L. J., and
311 Schultz, M. G.: Global modeling of tropospheric chemistry with assimilated meteorology: Model description and evaluation,
312 *J. Geophys. Res.-Atmos.*, 106, 23073–23095, <https://doi.org/10.1029/2001jd000807>, 2001.
- 313 Cai, W., Li, K., Liao, H., Wang, H., and Wu, L.: Weather conditions conducive to Beijing severe haze more frequent under
314 climate change, *Nat Clim Change*, 7, 257–262, 2017.
- 315 Chen, S., Guo, J., Song, L., Li, J., Liu, L., and Cohen, J.: Inter-annual variation of the spring haze pollution over the North
316 China Plain: Roles of atmospheric circulation and sea surface temperature, *Int. J. Climatol.*, 39, 783–798, 2019.
- 317 Cohen, A., Brauer, M., Burnett, R., Anderson, H., Frostad, J., Estep, K., Balakrishnan, K., Brunekreef, B., Dandona, L.,
318 Dandona, R., Feigin, V., Freedman, G., Hubbell, B., Jobling, A., Kan, H., Knibbs, L., Liu, Y., Martin, R., Morawska, L., Pope,
319 C., Shin, H., Straif, K., Shaddick, G., Thomas, M., Dingenen, R., Donkelaar, A., Vos, T., Murray, C., and Forouzanfar, M.:
320 Estimates and 25-year trends of the global burden of disease attributable to ambient air pollution: An analysis of data from the
321 Global Burden of Diseases Study 2015, *Lancet*, 389, 1907–1918, 2017.
- 322 Dang, R. and Liao, H.: Severe winter haze days in the Beijing-Tianjin-Hebei region from 1985 to 2017 and the roles of
323 anthropogenic emissions and meteorology, *Atmos. Chem. Phys.*, 19, 10801–10816, 2019.
- 324 Dee, D. P., Uppala, S. M., Simmons, A. J., Berrisford, P., Poli, P., Kobayashi, S., Andrae, U., Balmaseda, M. A., Balsamo,
325 G., Bauer, P., Bechtold, P., and Beljaars, A. C. M.: The ERA Interim reanalysis: configuration and performance of the data
326 assimilation system, *Q. J. Roy. Meteor. Soc.*, 137, 553–597, <https://doi.org/10.1002/qj.828>, 2011.
- 327 Ding, D. and Liu, Y.: Analysis of long-term variations of fog and haze in China in recent 50 years and their relations with
328 atmospheric humidity, *Sci. China Ser. D.*, 57, 36–46, 2014.

329 Gelaro, R., McCarty, W., Suarez, M. J., Todling, R., Molod, A., Takacs, L., Randles, C. A., Darmenov, A., Bosilovich, M. G.,
330 Reichle, R., Wargan, K., Coy, L., Cullather, R., Draper, C., Akella, S., Buchard, V., Conaty, A., da Silva, A. M., Gu, W., Kim,
331 G. K., Koster, R., Lucchesi, R., Merkova, D., Nielsen, J. E., Partyka, G., Pawson, S., Putman, W., Rienecker, M., Schubert, S. D.,
332 Sienkiewicz, M., and Zhao, B.: The Modern-Era Retrospective Analysis for Research and Applications, Version 2 (MERRA2),
333 *J. Climate*, 30, 5419–5454, <https://doi.org/10.1175/jcli-d-160758.1>, 2017.

334 He, C., Liu, R., Wang, X., Liu, S., Zhou, T., and Liao, W.: How does El Niño-Southern Oscillation modulate the interannual
335 variability of winter haze days over eastern China? *Sci. Total Environ.*, 651, 1892–1902, 2019.

336 Huug, D., Huang, J., and Fan, Y.: Performance and analysis of the constructed analogue method applied to US soil moisture
337 applied over 1981–2001, *J. Geophys. Res.*, 108, 1–16, 2003.

338 Horton, D., Skinner, C., Singh, D., Diffenbaugh, N.: Occurrence and persistence of future atmospheric stagnation events, *Nat.*
339 *Clim. Change*, 4, 698–703, 2014.

340 Kalnay, E., Kanamitsu, M., Kistler, R., Collins, W., Deaven, D., Gandin, L., Iredell, M., Saha, S., White, G., Woollen, J., Zhu,
341 Y., Leetmaa, A., Reynolds, R., Chelliah, M., Ebisuzaki, W., Higgins, W., Janowiak, J., Mo, K. C., Ropelewski, C., Wang, J.,
342 Jenne, R., and Joseph, D.: The NCEP/NCAR 40-year reanalysis project, *B. Am. Meteorol. Soc.*, 77, 437–471,
343 [https://doi.org/10.1175/1520-0477\(1996\)077<0437:TNYRP>2.0.CO;2](https://doi.org/10.1175/1520-0477(1996)077<0437:TNYRP>2.0.CO;2), 1996.

344 Li, K., Liao, H., Cai, W., and Yang, Y.: Attribution of anthropogenic influence on atmospheric patterns conducive to recent
345 most severe haze over eastern China, *Geophys. Res. Lett.*, 45, 2072–2081, 2018.

346 Li, M., Zhang, Q., Kurokawa, J.-I., Woo, J.-H., He, K., Lu, Z., Ohara, T., Song, Y., Streets, D. G., Carmichael, G. R., Cheng,
347 Y., Hong, C., Huo, H., Jiang, X., Kang, S., Liu, F., Su, H., and Zheng, B.: MIX: a mosaic Asian anthropogenic emission
348 inventory under the international collaboration framework of the MICS-Asia and HTAP, *Atmos. Chem. Phys.*, 17, 935–963,
349 <https://doi.org/10.5194/acp-17-935-2017>, 2017.

350 Liu, J., Wang, B., Cane, M., Yim, S., and Lee, J.: Divergent global precipitation changes induced by natural versus
351 anthropogenic forcing, *Nature*, 493, 656–659, 2013.

352 Lu, X., Lin, C., Li, W., Chen, Y., Huang, Y., Fung, J., and Lau, A.: Analysis of the adverse health effects of PM_{2.5} from 2001
353 to 2017 in China and the role of urbanization in aggravating the health burden, *Sci. Total Environ.*, 652, 683–695, 2019.

354 Mao, L., Liu, R., Liao, W., Wang, X., Shao, M., Liu, S., and Zhang, Y.: An observation-based perspective of winter haze days
355 in four major polluted regions of China, *Natl. Sci. Rev.*, 6, 515–523, 2019.

356 Mcvicar, T., Roderick, M., Donohue, R., Li, L., Niel, T., Thomas, A., Grieser, J., Jhajharia, D., Himri, Y., Mahowald, N.,
357 Mescherskaya, A., Kruger, A., Rehman, S., Dinpashoh, Y.: Global review and synthesis of trends in observed terrestrial near-
358 surface wind speeds: Implications for evaporation, *J Hydrol.*, 416, 182–205, 2012.

359 Ministry of Ecology and Environment of the People's Republic of China: Ambient air quality standards, China Environmental
360 Science Press, Beijing, 2012.

361 Niu, F., Li, Z., Li, C., Lee, K., and Wang, M.: Increase of wintertime fog in China: Potential impacts of weakening of the
362 Eastern Asian monsoon circulation and increasing aerosol loading, *J. Geophys. Res.*, 115, D7, 2010.

363 Park, R. J., Jacob, D. J., Field, B. D., Yantosca, R. M., and Chin, M.: Natural and transboundary pollution influences on sulfate-
364 nitrate-ammonium aerosols in the United States: Implications for policy, *J. Geophys. Res.-Atmos.*, 109, D15204,
365 <https://doi.org/10.1029/2003jd004473>, 2004.

366 Robinson, D. A., Dewey, K. F., and Heim Jr., R.: Global snow cover monitoring: an update, *B. Am. Meteorol. Soc.*, 74, 1689–
367 1696, 1993.

368 Shi, Y., Hu, F., Lü, R., and He, Y.: Characteristics of urban boundary layer in heavy haze process based on beijing 325m
369 tower data, *Atmos. Oceanic Sci. Lett.*, 12, 41–49, 2019.

370 Shi, X., Sun, J., Sun, Y., Bi, W., Zhou, X., and Yi, L.: The impact of the autumn Atlantic sea surface temperature three-pole
371 structure on winter atmospheric circulation, *Acta. Oceanol. Sin.*, 37, 33–40, 2015.

372 Shi, P., Zhang, G., Kong, F., Chen, D., Azorin-Molina, C., and Guijarro, J.: Variability of winter haze over the Beijing-Tianjin-
373 Hebei region tied to wind speed in the lower troposphere and particulate sources, *Atmos. Res.*, 215, 1–1, 2019.

374 Smith, T., Reynolds, R., Peterson, T., and Lawrimore, J.: Improvements to NOAA's historical merged land–ocean surface
375 temperature analysis (1880–2006), *J. Climate*, 21, 2283–2296, 2008.

376 Xiao, D., Li, Y., Fan, S., Zhang, R., Sun, J., and Wang, Y.: Plausible influence of Atlantic Ocean SST anomalies on winter
377 haze in China, *Theor. Appl. Climatol.*, 122, 249–257, 2015.

378 Yang, Y., Liao, H., and Lou, S.: Increase in winter haze over eastern China in recent decades: Roles of variations in
379 meteorological parameters and anthropogenic emissions, *J. Geophys. Res. Atmos.*, 121, 13050–13065, 2016.

380 Yin, Z. and Wang, H.: The relationship between the subtropical Western Pacific SST and haze over North-Central North China
381 Plain, *Int. J. Climatol.*, 36, 3479–3491, 2016a.

382 Yin, Z. and Wang, H.: Seasonal prediction of winter haze days in the north central North China Plain, *Atmos. Chem. Phys.*,
383 16, 14843–14852, 2016b.

384 Yin, Z., and Wang, H.: Role of atmospheric circulations in haze pollution in December 2016, *Atmos. Chem. Phys.*, 17, 11673–
385 11681, 2017.

386 Yin, Z. and Wang, H.: The strengthening relationship between Eurasian snow cover and December haze days in central North
387 China after the mid-1990s, *Atmos. Chem. Phys.*, 18, 4753–4763, 2018.

388 Yin, Z., and Zhang, Y.: Climate anomalies contributed to the rebound of PM_{2.5} in winter 2018 under intensified regional air
389 pollution preventions, *Sci. Total Environ.*, [726, 138514, 2020](https://doi.org/10.1016/j.scitotenv.2020.138514).

390 Yin, Z., Li, Y., and Wang, H.: Response of Early Winter Haze Days in the North China Plain to Autumn Beaufort Sea Ice.
391 Atmos. Chem. Phys., 19, 1439–1453, 2019.

392 Yin, Z., Wang, H., and Chen, H.: Understanding severe winter haze events in the North China Plain in 2014: Roles of climate
393 anomalies, Atmos. Chem. Phys., 17, 1641–1651, 2017.

394 Yin, Z., Wang, H., and Guo, W.: Climatic change features of fog and haze in winter over North China and Huang-Huai Area,
395 Sci. China Earth Sci., 58, 1370–1376, 2015.

396 Wang, H.: On assessing haze attribution and control measures in China, Atmos. Oceanic Sci. Lett., 11, 120–122, 2018.

397 Wang, H. and Chen, H.: Understanding the recent trend of haze pollution in eastern China: roles of climate change, Atmos.
398 Chem. Phys., 16, 4205–4211, 2016.

399 Wei, Y., Li, J., Wang, Z., Chen, H., Wu, Q., Li, J., Wang, Y., and Wang, W.: Trends of surface PM_{2.5} over Beijing–Tianjin–
400 Hebei in 2013–2015 and their causes: emission controls vs. meteorological conditions, Atmos. Oceanic Sci. Lett., 10, 276–
401 283, 2017.

402 Wilks, D.: Statistical methods in the atmospheric sciences, Academic press, Oxford, 2011.

403 Wu, P., Ding, Y., and Liu, Y.: Atmospheric circulation and dynamic mechanism for persistent haze events in the Beijing–
404 Tianjin–Hebei region, Adv. Atmos. Sci., 34, 429–440, 2017.

405 Zhang, Q. and Crooks, R.: Toward an environmentally sustainable future: Country environmental analysis of the People’s
406 Republic of China, China Financial and Economic Publishing House, Beijing, 2012.

407 Zhao, S., Li, J., and Sun, C.: Decadal variability in the occurrence of wintertime haze in central eastern China tied to the Pacific
408 Decadal Oscillation, Sci. Rep., 6, 27424, 2016.

409 Zhong, W., Yin, Z., and Wang, H.: The Relationship between the Anticyclonic Anomalies in Northeast Asia and Severe Haze
410 in the Beijing-Tianjin-Hebei Region, Atmos. Chem. Phys., 19, 5941–5957, 2019.

411 Zou, Y., Wang, Y., Zhang, Y., and Koo, J.: Arctic sea ice, Eurasia snow, and extreme winter haze in China, Sci. Adv., 3,
412 e1602751, 2017.

413 **Table and Figure legends**

414 Table 1. Correlation coefficients (CCs) between HD_{NC} and the SST_P, SST_A, Snow_c and Soil_w indices after detrending and the
415 trends of the SST_P, SST_A, Snow_c and Soil_w indices for the periods 1991–2010 and 2010–2018. CC₁, CC₂, and CC₃ represent
416 the correlation coefficients from 1979 to 2018, 1979 to 2010 and 2010 to 2018, respectively. “****” indicates that the CC was
417 above the 99% confidence level, “***” indicates that the CC was above the 95% confidence level, and “**” indicates that the
418 CC was above the 90% confidence level.

419 Table 2. The contribution rate of fitted HD_{NC} and each external forcing factor to the trend of HD_{NC} in P1 and P2, respectively.

420 Figure 1. (a) Variations in the December-January emissions (unit: Tg) of black carbon (BC), ammonia (NH₃), nitrogen oxide
421 (NO_x), organic carbon (OC), sulfur dioxide (SO₂), PM₁₀ and PM_{2.5} over North China from 1979 to 2013 and the variation in
422 HD_{NC} from 1979 to 2018 (black solid line). The blue and green solid (dashed) lines indicate the number of days when the
423 hourly PM_{2.5} concentrations in a day exceeded 75 μg m⁻³ and 100 μg m⁻³, respectively, from 2009 to 2016 (2014 to 2018)
424 using Beijing (North China) observed data from the US embassy (China National Environmental Monitoring Centre). (b)
425 Temporal evolutions of HD_{NC} (in black), simulated haze days (unit: days; red) in NC. The dashed lines denote linear
426 regressions for 1991–2010 (P1) and 2010–2018 (P2). The black and red Trend 1 and Trend 2 represent the linear trends of the
427 observed and simulated haze days in P1 and P2, respectively.

428 Figure 2. Area-averaged linear trends of the BLH (unit: m/yr), specific humidity (unit: %/10 yr), surface wind speed (unit: m
429 s⁻¹/10² yr) and omega (unit: pascal s⁻¹/10³ yr) over NC in early winter for the periods 1991–2010 (P1) and 2010–2018 (P2).
430 All datasets were 5-year running averages before calculating the trends.

431 Figure 3. Linear trends of the Pacific and Atlantic SST (unit: °C/yr; a, b), Eurasian snow cover (unit: %/yr; c, d), and central
432 Siberian soil moisture (unit: mm/yr; e, f) for the periods 1991–2010 (P1) and 2010–2018 (P2). All datasets were 5-year running
433 averages before calculating the trends. The green boxes represent the regions where the four indices are defined. Black dots
434 indicate that the trends were above the 95% confidence level.

435 Figure 4. Variations in HD_{NC} (in black) and the SST_P (unit: °C; a, red), SST_A (unit: °C; b, blue), Snowc (unit: %; c, yellow),
436 and Soilw (unit: mm; d, green) indices and the HD_{NC} values fitted by the MLR model by the above four factors (unit: days; e,
437 purple) from 1979 to 2018. Thick lines indicate 5-year running averaged time series. The rectangles and triangles indicate the
438 inflection points of HD_{NC} and the four indices, which were tested by the Mann-Kendall test.

439 Figure 5. Composite of the simulated HD_{NC} caused by the four external forcing factors (Favor Years minus Unfavor Years).
440 The circles and crosses represent the original and detrended sequences, respectively.

441

444 **Table 1.** Correlation coefficients (CCs) between HD_{NC} and the SST_P , SST_A , $Snowc$ and $Soilw$ indices after detrending and the
 445 trends of the SST_P , SST_A , $Snowc$ and $Soilw$ indices for the periods 1991–2010 and 2010–2018. CC_1 , CC_2 , and CC_3 represent
 446 the correlation coefficients from 1979 to 2018, 1979 to 2010 and 2010 to 2018, respectively. “***” indicates that the CC was
 447 above the 99% confidence level, “**” indicates that the CC was above the 95% confidence level, and “*” indicates that the
 448 CC was above the 90% confidence level.

449

	CC with HD_{NC}	Trend / 10yr	
		1991–2010	2010–2018
SST_P	$CC_1 = 0.67$ ***	–0.20 °C***	1.99 °C***
	$CC_2 = 0.39$ **		
	$CC_3 = 0.66$ ***		
SST_A	$CC_1 = -0.64$ ***	0.55 °C***	–0.52 °C***
	$CC_2 = -0.54$ ***		
	$CC_3 = -0.61$ ***		
$Snowc$	$CC_1 = 0.54$ ***	–1.79% **	28.35% ***
	$CC_2 = 0.46$ ***		
	$CC_3 = 0.53$ ***		
$Soilw$	$CC_1 = -0.60$ ***	38.78mm***	–51.81mm***
	$CC_2 = -0.30$ *		
	$CC_3 = -0.66$ ***		

450

451 **Table 2.** The contribution rate of fitted HD_{NC} and each external forcing factor to the trend of HD_{NC} in P1 and P2,
 452 respectively.

	Fitted HD_{NC}	SST_P	SST_A	$Snowc$	$Soilw$
P1	112.2%	23.3%	43.9%	4.5%	40.7%
P2	72.3%	41.9%	7.5%	12.9%	10.0%

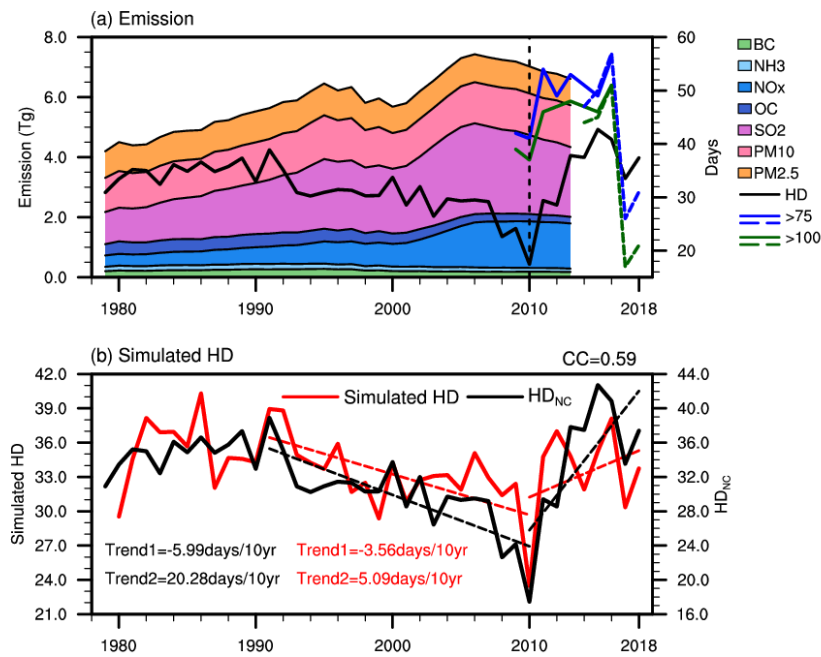
453

454

455

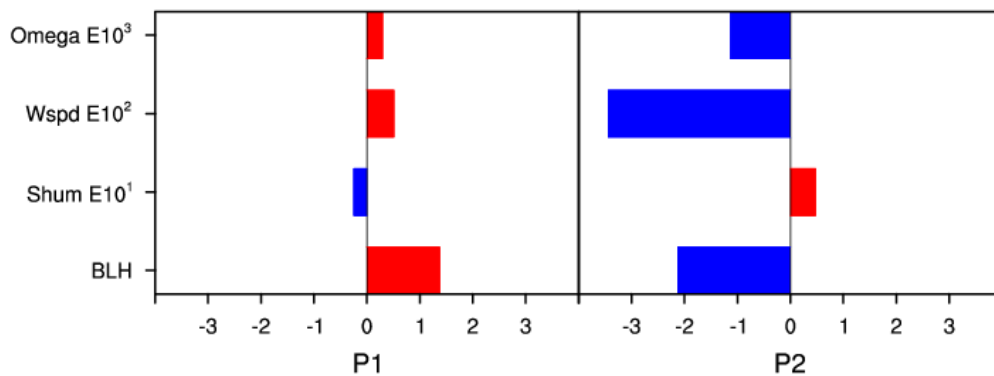
456

457



460

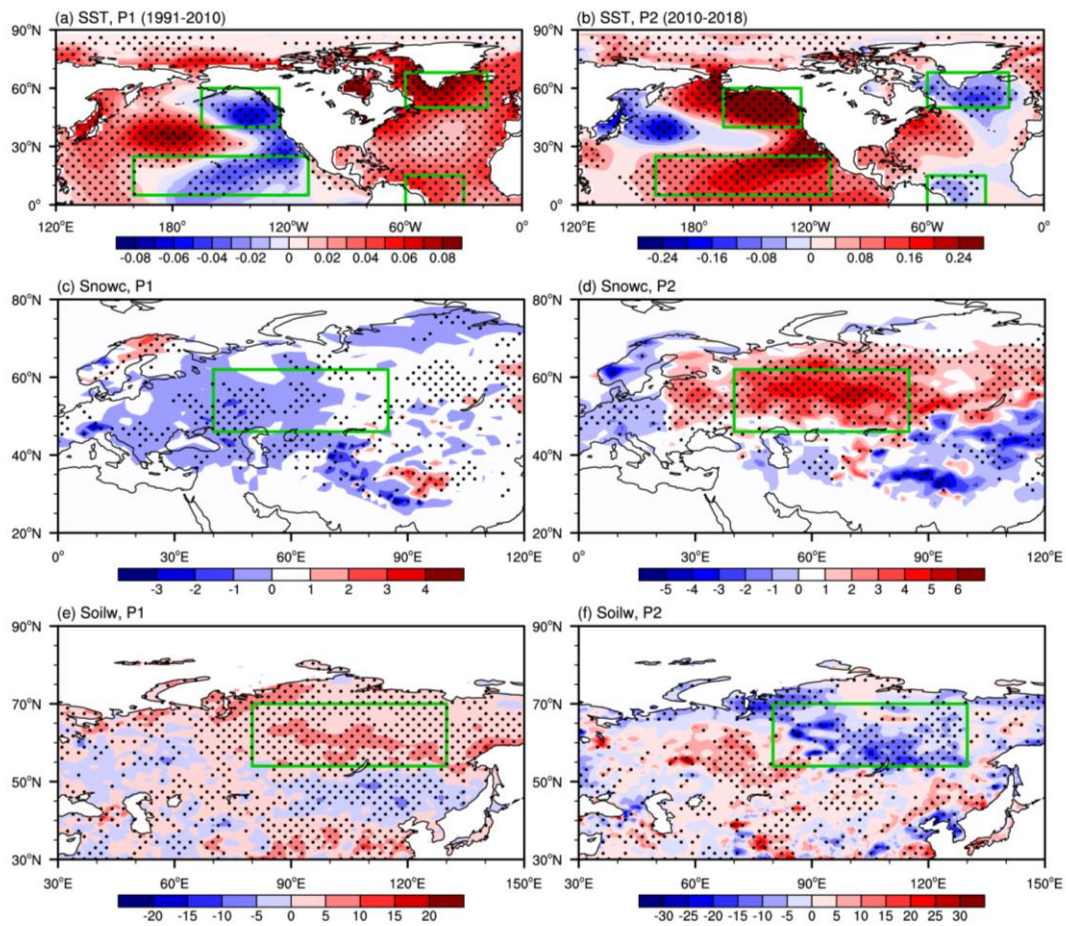
461 **Figure 1.** (a) Variations in the December-January emissions (unit: Tg) of black carbon (BC), ammonia (NH₃), nitrogen oxide
 462 (NO_x), organic carbon (OC), sulfur dioxide (SO₂), PM₁₀ and PM_{2.5} over North China from 1979 to 2013 and the variation in
 463 HD_{NC} from 1979 to 2018 (black solid line). The blue and green solid (dashed) lines indicate the number of days when the
 464 hourly PM_{2.5} concentrations in a day exceeded 75 $\mu\text{g m}^{-3}$ and 100 $\mu\text{g m}^{-3}$, respectively, from 2009 to 2016 (2014 to 2018)
 465 using Beijing (North China) observed data from the US embassy (China National Environmental Monitoring Centre). (b)
 466 Temporal evolutions of HD_{NC} (in black), simulated haze days (unit: days; red) in NC. The dashed lines denote linear
 467 regressions for 1991–2010 (P1) and 2010–2018 (P2). The black and red Trend 1 and Trend 2 represent the linear trends of the
 468 observed and simulated haze days in P1 and P2, respectively.



469

470 **Figure 2.** Area-averaged linear trends of the BLH (unit: m/yr), specific humidity (unit: %/10 yr), surface wind speed (unit: m
 471 $\text{s}^{-1}/10^2 \text{ yr}$) and omega (unit: pascal $\text{s}^{-1}/10^3 \text{ yr}$) over NC in early winter for the periods 1991–2010 (P1) and 2010–2018 (P2).

472 All datasets were 5-year running averages before calculating the trends.



474

475

476

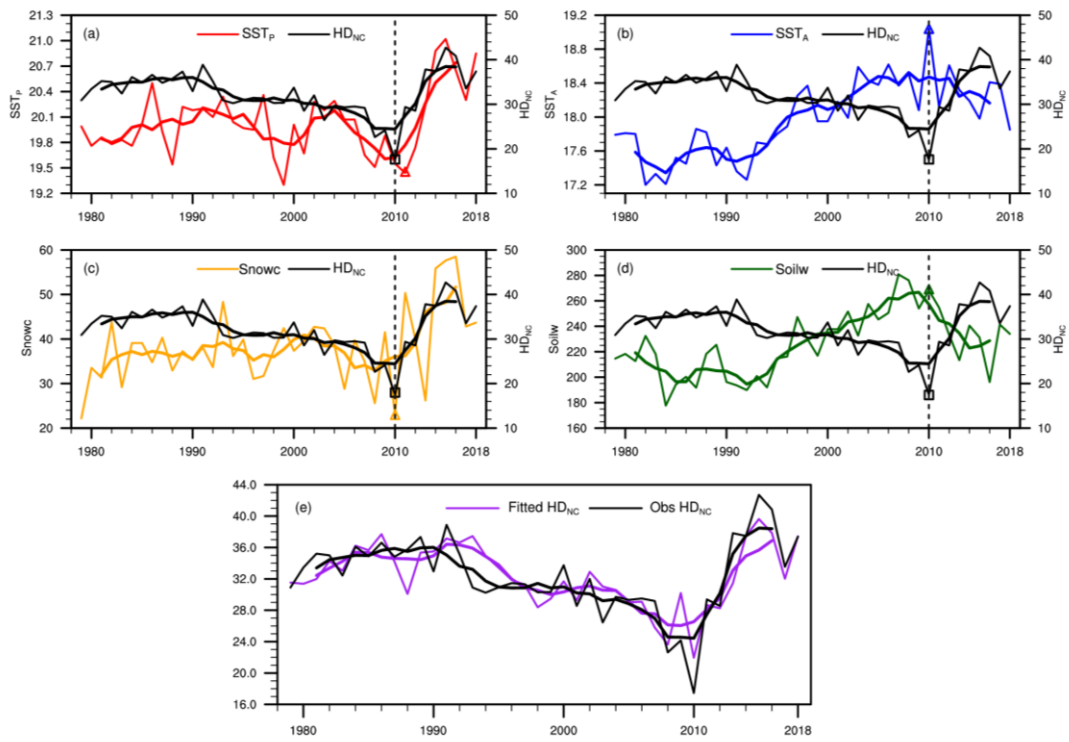
477

478

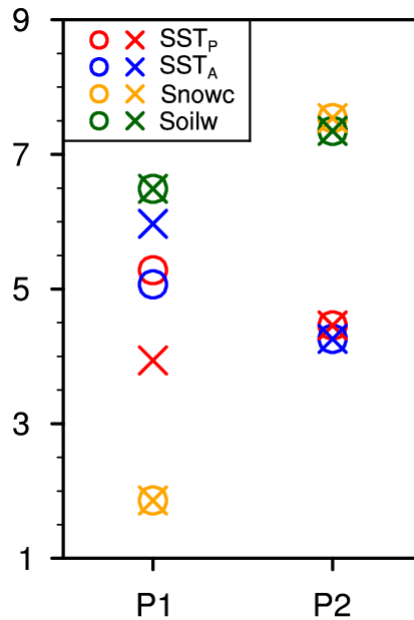
479

480

Figure 3. Linear trends of the Pacific and Atlantic SST (unit: $^{\circ}\text{C}/\text{yr}$; a, b), Eurasian snow cover (unit: $\%/\text{yr}$; c, d), and central Siberian soil moisture (unit: mm/yr ; e, f) for the periods 1991–2010 (P1) and 2010–2018 (P2). All datasets were 5-year running averages before calculating the trends. The green boxes represent the regions where the four indices are defined. Black dots indicate that the trends were above the 95% confidence level.



481
 482 **Figure 4.** Variations in HD_{NC} (in black) and the SST_P (unit: $^{\circ}C$; a, red), SST_A (unit: $^{\circ}C$; b, blue), $Snowc$ (unit: %; c, yellow),
 483 and $Soilw$ (unit: mm; d, green) indices and the HD_{NC} values fitted by the MLR model by the above four factors (unit: days;
 484 e, purple) from 1979 to 2018. Thick lines indicate 5-year running averaged time series. The rectangles and triangles indicate
 485 the inflection points of HD_{NC} and the four indices, which were tested by the Mann-Kendall test.



486
 487 **Figure 5.** Composite of the simulated HD_{NC} caused by the four external forcing factors (Favor Years minus Unfavor Years).
 488 The circles and crosses represent the original and detrended sequences, respectively.
 489